# Performance Analysis of Closed-Form, ESPRIT Based 2-D Angle Estimator for Rectangular Arrays

Cherian P. Mathews, Martin Haardt, and Michael D. Zoltowski

*Abstract*—**The 2-D DFT beamspace ESPRIT is a recently developed algorithm for use in conjunction with uniform rectangular arrays (URA's) that provides automatically paired azimuth and elevation angle estimates of incident signals via a closed-form procedure. This letter investigates the statistical performance of 2D DFT beamspace ESPRIT. Expressions for the 2D DFT beamspace ESPRIT estimator variances are obtained. Samples variances of the azimuth and elevation angle estimates obtained through Monte Carlo simulations are shown to be in close agreement with theoretically predicted variances.**

## I. Introduction

THE 2-D DFT beamspace ESPRIT is a recently developed algorithm [1]–[3] for use with uniform rectangular arrays (URA's) that provides automatically paired source azimuth and elevation angle estimates via a closed-form procedure. The algorithm provides 2-D angle estimates without requiring expensive search procedures or employing *ad hoc* pairing procedures. Further, the algorithm does not break down if several sources have a common bearing relative to one of the array axes. Reduced dimensional beamspace processing provides a further reduction in the computational demands of the algorithm. This paper investigates the statistical performance of 2-D DFT beamspace ESPRIT. Asymptotic expressions for the variances of the 2-D DFT beamspace ESPRIT DOA estimators are obtained. Computer simulations showing agreement between the experimental and theoretical results are presented. The performance analysis results also apply to 2-D unitary ESPRIT [2,3], the element space counterpart of 2-D DFT beamspace ESPRIT.

## II. Summary of 2-D DFT Beamspace ESPRIT

The array geometry involves a URA of $M \times N$ sensors located in the $xy$ plane, with the array centroid located at the origin. The array elements parallel to the $x$ axis are spaced $\Delta_x$ apart, and those parallel to the $y$ axis are spaced $\Delta_y$ apart.

The DOA of a source is specified by the pair $(u, v)$, where $u = \sin\theta\cos\phi$ and $v = \sin\theta\sin\phi$ are the direction cosines with respect to the $x$ and $y$ axes, respectively. When a narrowband source (of wavelength $\lambda$) impinges on the array from the direction $(u, v)$, the phase shifts between successive elements along the $x$ and $y$ axes are $\mu = 2\pi\frac{\Delta_x}{\lambda}u$ and $\nu = 2\pi\frac{\Delta_y}{\lambda}v$, respectively. Note that $\mu$ and $\nu$ lie in the range $[-\pi, \pi]$ when $\Delta_x = \Delta_y = \lambda/2$.

The array output is modeled as $\mathbf{x}(t) = \mathbf{A}\mathbf{s}(t) + \mathbf{n}(t)$, where $\mathbf{x}(t)$ is the $MN$ vector formed by stacking the columns of the URA outputs, $\mathbf{A}$ is the $MN \times d$ DOA matrix (assuming d incident sources), $\mathbf{s}(t)$ is the vector of signal complex envelopes at the origin, and $\mathbf{n}(t)$ is the stacked noise vector. The columns of $\mathbf{A}$ have the form $\mathrm{vec}[\mathbf{a}_M(\mu)\mathbf{a}_N^T(\nu)]$, where $\mathrm{vec}(\cdot)$ denotes the column stacking operator, and $\mathbf{a}_M(\mu) = e^{-j\frac{M-1}{2}\mu}[1, e^{j\mu}, \cdots, e^{j(M-1)\mu}]^T$. 2-D DFT beamspace ESPRIT is summarized below followed by an explanation of pertinent points. ($\otimes$ denotes the Kronecker matrix product below.)

1) Construct $\hat{\mathbf{R}}_\mathbf{y} = \frac{1}{K}\sum_{k=1}^{K}\mathbf{y}(k)\mathbf{y}^H(k)$, where $\mathbf{y}(k) = \mathbf{F}^H\mathbf{x}(k)$ and $\mathbf{F}^H = \mathbf{W}_{B_y}^{(n)H} \otimes \mathbf{W}_{B_x}^{(m)H}$.
2) Perform an EVD of $\hat{\mathbf{R}} = \mathrm{Re}\{\hat{\mathbf{R}}_\mathbf{y}\}$ and obtain an estimate of the number of sources, $\hat{d}$, in the sector. Obtain the beamspace signal subspace estimate $\hat{\mathbf{S}}$ via the $\hat{d}$ "largest" eigenvectors of $\hat{\mathbf{R}}$.
3) Obtain $\hat{\mathbf{\Psi}}_\mu$ and $\hat{\mathbf{\Psi}}_\nu$ as the least squares (or total least squares) solutions to the real-valued systems of equations $\mathbf{\Gamma}_{\mu 1}\hat{\mathbf{S}}\mathbf{\Psi}_\mu = \mathbf{\Gamma}_{\mu 2}\hat{\mathbf{S}}$, and $\mathbf{\Gamma}_{\nu 1}\hat{\mathbf{S}}\mathbf{\Psi}_\nu = \mathbf{\Gamma}_{\nu 2}\hat{\mathbf{S}}$.
4) Perform an EVD of $\hat{\mathbf{\Psi}} = \hat{\mathbf{\Psi}}_\mu + j\hat{\mathbf{\Psi}}_\nu$. The eigenvalues of $\hat{\mathbf{\Psi}}$ are $\hat{\lambda}_i = \hat{\omega}_i + j\hat{\delta}_i$, where $\hat{\omega}_i = \tan(\hat{\mu}_i/2)$ and $\hat{\delta}_i = \tan(\hat{\nu}_i/2)$. We thus have $\hat{u}_i = \lambda/(\pi\Delta_x)\tan^{-1}(\hat{\omega}_i)$, and $\hat{v}_i = \lambda/(\pi\Delta_y)\tan^{-1}(\hat{\delta}_i)$.

The beamforming matrix $\mathbf{F}^H$ in step 1 synthesizes $B_xB_y$ 2D DFT beams. $B_x$ consecutive beams (beginning at beam $m \in [0, M-1]$) are formed along $\mu$, and $B_y$ consecutive beams (beginning at beam $n \in [0, N-1]$) are formed along $\nu$. We have $\mathbf{W}_{B_x}^{(m)} = [\mathbf{a}_M(2\pi m/M) \vdots \mathbf{a}_M(2\pi(m+1)/M) \vdots \cdots \vdots \mathbf{a}_M(2\pi(m+B_x-1)/M)]$ and $\mathbf{W}_{B_y}^{(n)} = [\mathbf{a}_N(2\pi n/N) \vdots \mathbf{a}_N(2\pi(n+1)/N) \vdots \cdots \vdots \mathbf{a}_N(2\pi(n+B_y-1)/N)]$. The rows of $\mathbf{W}_{B_x}^{(m)H}$ are scaled $M$-point DFT weight vectors corresponding to bins $m, m+1, \cdots, m+B_x-1$ (computed modulo $M$). The rows of $\mathbf{W}_{B_y}^{(n)H}$ have a similar interpretation. The beamformer $\mathbf{F}^H$ thus narrows the scope of the search for sources to the spatial sector roughly specified by $2\pi m/M \le \mu \le 2\pi(m+B_x-1)/M$, $2\pi n/N \le \nu \le$

Manuscript received July 28, 1995. This work was supported by the National Science Foundation under Grant MIP-9320890 and by AFOSR under Contract F49620-95-1-0451. The associate editor coordinating the review of this letter and approving it for publication was Prof. J. M. F. Moura.

C. P. Mathews is with the UF/UWF Joint EE Program, Bldg. 70, University of West Florida, Pensacola, FL 32514-5751 USA.

M. Haardt is with the Institute of Network Theory and Circuit Design, Technical University of Munich, D-80290 Munich, Germany.

M. D. Zoltowski is with the School of Electrical and Computer Engineering, 1285 Electrical Engineering Bldg., Purdue University, West Lafayette, IN 47907 USA (e-mail: mikedz@ecn.purdue.edu).

Publisher Item Identifier S 1070-9908(96)03254-3.

$2\pi(n + B_y - 1)/N$. Note also that a steering angle $\alpha > \pi$ (along $\mu$ or $\nu$) is identical to a steering angle $\alpha - 2\pi$.

The equations in step 3 follow from a relationship between any two adjacent 2-D DFT beams (adjacency in $\mu$ or $\nu$). The matrices $\mathbf{\Gamma}_M^c$ and $\mathbf{\Gamma}_M^s$ defined, at the bottom of the page, summarize these relationships. Row $i$ of these matrices give the relationship between the $i$th and $(i+1)$th beams (modulo $M$). For the case of reduced dimension beamspace processing form: $\mathbf{\Gamma}_1 = \mathbf{J}_{B_x-1}^{(m)} \mathbf{\Gamma}_M^c \mathbf{J}_{B_x}^{(m)T}$, $\mathbf{\Gamma}_2 = \mathbf{J}_{B_x-1}^{(m)} \mathbf{\Gamma}_M^s \mathbf{J}_{B_x}^{(m)T}$, $\mathbf{\Gamma}_3 = \mathbf{J}_{B_y-1}^{(n)} \mathbf{\Gamma}_N^c \mathbf{J}_{B_y}^{(n)T}$, and $\mathbf{\Gamma}_4 = \mathbf{J}_{B_y-1}^{(n)} \mathbf{\Gamma}_N^s \mathbf{J}_{B_y}^{(n)T}$. Here $\mathbf{J}_{B_x}^{(m)}$ denotes a selection matrix that picks out $B_x$ consecutive rows from the matrix it operates on (beginning with row $m$). Note again that the last row (row $M-1$) is followed by the first row (row 0). The matrices needed for step 3 are constructed as follows: $\mathbf{\Gamma}_{\mu 1} = \mathbf{I}_{B_y} \otimes \mathbf{\Gamma}_1$, $\mathbf{\Gamma}_{\mu 2} = \mathbf{I}_{B_y} \otimes \mathbf{\Gamma}_2$, $\mathbf{\Gamma}_{\nu 1} = \mathbf{\Gamma}_3 \otimes \mathbf{I}_{B_x}$, and $\mathbf{\Gamma}_{\nu 2} = \mathbf{\Gamma}_4 \otimes \mathbf{I}_{B_x}$. 2-D unitary ESPRIT [2,3] is similar to 2-D DFT beamspace ESPRIT except that it employs a different (sparse) transformation matrix $\mathbf{F}^H$ and thus different selection matrices instead of the $\mathbf{\Gamma}_{(\cdot)}$ of step 3, and that these matrices have full dimension. The performance analysis below applies to 2-D unitary ESPRIT with minor changes.

## III. Performance Analysis

The analysis of 2-D DFT beamspace ESPRIT presented below follows the analysis of UCA-ESPRIT [4]. In [4] it is shown that the error free matrix $\mathbf{\Psi} = \mathbf{\Psi}_\mu + j\mathbf{\Psi}_\nu$ has the spectral decomposition, where $\mathbf{\Psi} = \mathbf{T}^{-1}(\mathbf{\Omega}_\mu + j\mathbf{\Omega}_\nu)\mathbf{T}$, $\mathbf{\Omega}_\mu + j\mathbf{\Omega}_\nu$ is the diagonal matrix whose elements are the eigenvalues $\lambda_i = \omega_i + j\delta_i, i = 1, ..., d$, and $\mathbf{T}$ is real-valued. Thus $\mathbf{\Psi}_\mu$ and $\mathbf{\Psi}_\nu$ have a common set of real-valued eigenvectors given by the columns of $\mathbf{T}^{-1}$. Let the left and right eigenvectors of $\mathbf{\Psi}$ be denoted as $\mathbf{q}_i^T$ and $\mathbf{x}_i = [x_{i1}, x_{i2}, ..., x_{id}]^T$, respectively. The columns of the matrices $\mathbf{S}$ and $\mathbf{G}$ are the signal eigenvectors, $\mathbf{s}_i$, and noise eigenvectors, $\mathbf{g}_i$, respectively, of $\mathbf{R}$. Let $l_i, i = 1, \cdots, d$, denote the $d$ largest eigenvalues of $\mathbf{R}$, and $\sigma$ be the noise power (the noise is assumed to be Gaussian and spatially and temporally white). The signal eigenvector estimation errors $\mathbf{s}_i^e = \hat{\mathbf{s}}_i - \mathbf{s}_i$ are asymptotically (for large number of snapshots $K$) zero mean with covariance matrices given by [4] $\mathrm{Cov}(\mathbf{s}_i^e, \mathbf{s}_j^e) = \mathrm{E}[\mathbf{s}_i^e \mathbf{s}_j^{eT}] = \frac{1}{K} \sum_{r=1}^{d} \sum_{\substack{s=1 \\ s \neq j}}^{d} \frac{\Gamma_{rsji}}{(l_i - l_r)(l_j - l_s)} \mathbf{s}_r \mathbf{s}_s^T + \frac{1}{K} \frac{l_i \sigma}{2(l_i - \sigma)^2} \mathbf{G}\mathbf{G}^T \delta_{ij}$,

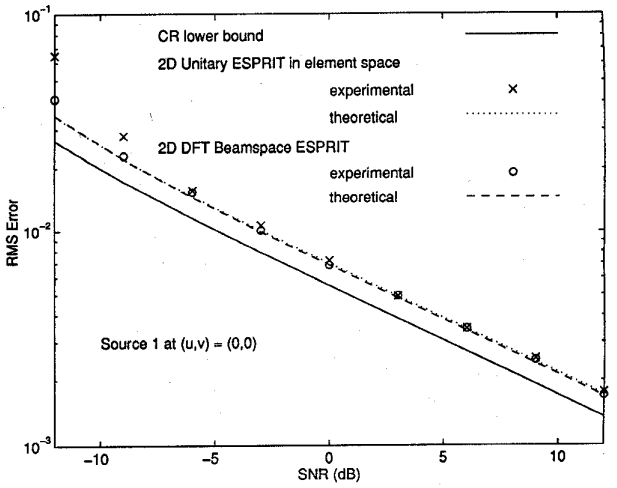


(a)

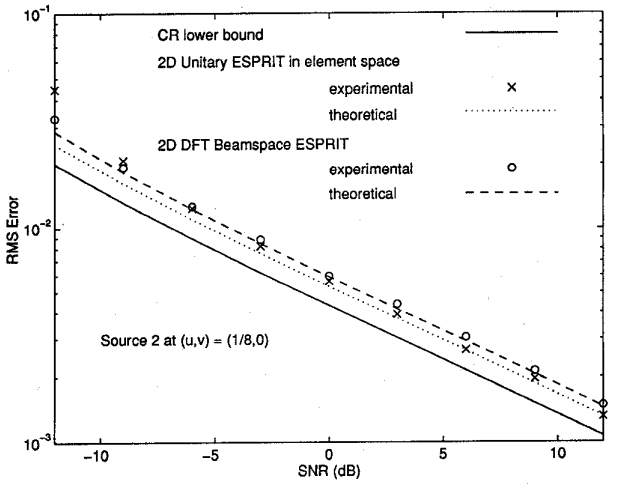


(b)

Fig. 1. Theoretical performance and Monte Carlo simulation results for 2-D DFT beamspace ESPRIT and 2-D unitary ESPRIT with 8×8 URA ($\Delta_x \Delta_y = \lambda/2$) and $d = 3$ sources at $(u_1, v_1) = (0, 0)$, $(u_2, v_2) = (1/8, 0)$, and $(u_3, v_3) = (0, 1/8)$. (a) Source 1 at $(u_1, v_1) = (0, 0)$. (b) Source 2 at $(u_2, v_2) = m(1/8, 0)$.

where $\delta_{ij}$ denotes the Kronecker delta, $\Gamma_{rsji} = \frac{1}{2}\{l_i l_s \cdot \delta_{ij}\delta_{rs} + l_i l_j \delta_{is}\delta_{jr} + \mathbf{w}_r^T(\mathbf{s}_s \mathbf{s}_j^T + \mathbf{s}_j \mathbf{s}_s^T)\mathbf{w}_i\}$ and $\mathbf{w}_i =$

$$\mathbf{\Gamma}_M^c = \begin{bmatrix} 1 & \cos(\pi/M) & 0 & \cdots & 0 & 0 \\ 0 & \cos(\pi/M) & \cos(2\pi/M) & \cdots & 0 & 0 \\ \vdots & \vdots & \vdots & \ddots & \vdots & \vdots \\ 0 & 0 & 0 & \cdots & \cos[(M-2)\pi/M] & \cos[(M-1)\pi/M] \\ (-1)^M & 0 & 0 & \cdots & 0 & \cos[(M-1)\pi/M] \end{bmatrix}$$

$$\mathbf{\Gamma}_M^s = \begin{bmatrix} 0 & \sin(\pi/M) & 0 & \cdots & 0 & 0 \\ 0 & \sin(\pi/M) & \sin(2\pi/M) & \cdots & 0 & 0 \\ \vdots & \vdots & \vdots & \ddots & \vdots & \vdots \\ 0 & 0 & 0 & \cdots & \sin[(M-2)\pi/M] & \sin[(M-1)\pi/M] \\ 0 & 0 & 0 & \cdots & 0 & \sin[(M-1)\pi/M] \end{bmatrix}$$

$\mathrm{Im}\{\mathbf{F}^H\mathbf{R}_{\mathbf{x}}\mathbf{F}\}\mathbf{s}_i$. The theorem below, proved along lines of a similar theorem in [4], gives asymptotic expressions for the variances/covariance of the 2-D DFT beamspace ESPRIT estimators $\hat{\omega}_i$ and $\hat{\delta}_i$. Approximate expressions for the variances of the direction cosine estimators $\hat{u}_i$ and $\hat{v}_i$ were derived based on $\hat{\omega}_i$ and $\hat{\delta}_i$ being concentrated about their true values. Details are not included here due to space limitations.

*Theorem 3.1:* The 2-D DFT beamspace ESPRIT estimators $\hat{\omega}_i$ and $\hat{\delta}_i$ are asymptotically unbiased with asymptotic variances/covariance expressed as follows (superscript † denotes Moore–Penrose pseudo-inverse):

$$\begin{aligned} &\mathrm{var}\,(\hat{\omega}_i) = \boldsymbol{\alpha}_{iR}^T\,\mathbf{H}_i\,\boldsymbol{\alpha}_{iR},\ \mathrm{var}\,(\hat{\delta}_i) = \boldsymbol{\alpha}_{iI}^T\,\mathbf{H}_i\,\boldsymbol{\alpha}_{iI}, \\ &\qquad \text{and } \mathrm{cov}\,(\hat{\omega}_i,\hat{\delta}_i) = \boldsymbol{\alpha}_{iR}^T\,\mathbf{H}_i\,\boldsymbol{\alpha}_{iI} \end{aligned} \tag{1}$$

where $\mathbf{H}_i = \sum_{j=1}^{d}\sum_{k=1}^{d} x_{ij}x_{ik}\,cov(\mathbf{s}_j^e,\mathbf{s}_k^e)$, $\boldsymbol{\alpha}_{iR}^T = \mathbf{q}_i^T(\boldsymbol{\Gamma}_{\mu 1}\mathbf{S})^{\dagger}(\boldsymbol{\Gamma}_{\mu 2} - \omega_i\boldsymbol{\Gamma}_{\mu 1})$, and $\boldsymbol{\alpha}_{iI}^T = \mathbf{q}_i^T(\boldsymbol{\Gamma}_{\nu 1}\mathbf{S})^{\dagger}(\boldsymbol{\Gamma}_{\nu 2} - \delta_i\boldsymbol{\Gamma}_{\nu 1})$. The direction cosine estimator variances are given by

$$\begin{aligned} \mathrm{Var}\,(\hat{u}_i) &\approx \left[\frac{\lambda}{\pi\Delta_x(1+\omega^2)}\right]^2 \mathrm{Var}\,(\hat{\omega}_i), \\ \mathrm{Var}\,(\hat{v}_i) &\approx \left[\frac{\lambda}{\pi\Delta_y(1+\delta^2)}\right]^2 \mathrm{Var}\,(\hat{\delta}_i). \end{aligned} \tag{2}$$

## IV. Results of Computer Simulations

An 8×8 URA ($M = N = 8$) with $\Delta_x = \Delta_y = \lambda/2$ was employed. The source scenario consisted of $d = 3$ equipowered uncorrelated sources at $(u_1, v_1) = (0,0)$, $(u_2, v_2) = (1/8, 0)$, and $(u_3, v_3) = (0, 1/8)$ corresponding to a mutual separation of a half-beamwidth. $K = 64$ snapshots were employed in each of $T = 1000$ independent trials. The root mean square error (RMSE) was employed as the performance metric: $\hat{RMSE}_i = \sqrt{\frac{1}{T}\sum_{t=1}^{T}\{(\hat{u}_{i_t} - u_i)^2 + (\hat{v}_{i_t} - v_i)^2\}}$, where $(\hat{u}_{i_t}, \hat{v}_{i_t})$ are the direction cosine estimates of the $i$th source in the $t$th trial. 2-D DFT beamspace ESPRIT was implemented with a set of 9 beams (3×3) with mainlobes centered at $(u, v) = (0, 0)$ . The RMSE's of 2-D DFT beamspace ESPRIT for sources 1 and 2 are plotted together with the theoretical performance curves in Fig. 1(a) and (b), respectively (curves for source 3 are similar and thus not included). Observe that the empirical RMSE's closely follow the theoretical predictions, except for deviations at low SNR's. Performance curves for 2-D unitary ESPRIT are also depicted. The performance of 2-D DFT beamspace ESPRIT is observed to be comparable to that of 2-D unitary ESPRIT. However, the former requires significantly less computation than the latter; it operates in 9-D beamspace as opposed to 64-D element space.

## References


[1] M. D. Zoltowski, M. Haardt, and C. P. Mathews, "Closed-form 2D angle estimation with rectangular arrays via DFT beamspace ESPRIT," in *28th Asilomar IEEE Conf. Signals, Systems, and Computers*, 1994, pp. 682–687.

[2] M. Haardt, M. D. Zoltowski, C. P. Mathews, and J. A. Nossek, "2D unitary ESPRIT for efficient 2D parameter estimation," in *Proc. IEEE Int. Conf. Acoust., Speech, Signal Processing*, 1995, pp. 2096–2099.

[3] M. D. Zoltowski, M. Haardt, and C. P. Mathews, "Closed-form 2D angle estimation with rectangular arrays in element space or beamspace via unitary ESPRIT," *IEEE Trans. Signal Processing*, vol. 44, pp. 326–328, Feb. 1996.

[4] C. P. Mathews and M. D. Zoltowski, "Performance analysis of the UCA-ESPRIT algorithm for circular ring arrays," *IEEE Trans. Signal Processing*, vol. 42, pp. 2535–2539, Sept. 1994.